Latest Data Constraint of Some Parameterized Dark Energy Models

Jing Yang, Xin-Yan Fan, Chao-Jun Feng*, and Xiang-Hua Zhai*

Division of Mathematica and Theoretical Physics, Shanghai Normal University, Shanghai 200234, China

(Received 30 September 2022; accepted manuscript online 23 November 2022)

Using various latest cosmological datasets including type-Ia supernovae, cosmic microwave background radiation, baryon acoustic oscillations, and estimations of the Hubble parameter, we test some dark-energy models with parameterized equations of state and try to distinguish or select observation-preferred models. We obtain the best fitting results of the six models and calculate their values of the Akaike information criteria and Bayes information criterion. We can distinguish these dark energy models from each other by using these two information criterions. However, the ΛCDM model remains the best fit model. Furthermore, we perform geometric diagnostics including statefinder and Om diagnostics to understand the geometric behavior of the dark energy models. We find that the six dark-energy models can be distinguished from each other and from ΛCDM, Chaplygin gas, quintessence models after the statefinder and Om diagnostics are performed. Finally, we consider the growth factor of the dark-energy models with comparison to the ΛCDM model. Still, we find the models can be distinguished from each other and from the ΛCDM model through the growth factor approximation.

DOI: 10.1088/0256-307X/40/1/019801

At the end of the 20th century, the observations of type-Ia supernovae (SNIa) first indicated that the universe is under accelerating expansion.[1,2] Later, various experimental observations, including the large-scale structure (LSS)[3,4] and the cosmic microwave background radiation (CMB),[5–10] also provided evidence for the accelerating expansion of the universe. In order to explain the acceleration of the universe, the efforts that continue to date include two aspects. On the one hand, the gravitational part may be modified, and extended theories of gravity may be constructed.[11–14] On the other hand, a matter component with negative pressure, i.e., dark energy (DE), which may drive the acceleration, is introduced into the matter part (see review articles on DE, Refs. [15–23]). The currently preferable and also the simplest cosmological model is the Λ cold dark matter (ΛCDM) model, in which the cosmological constant Λ plays the role of DE. However, due to the deficiencies of the ΛCDM model such as the cosmic coincidence issue and fine-tuning problem,[24–28] the dynamical DE models have been widely discussed.[29–38]

Due to the fact that there is no preferable DE model that can completely describe the dynamical phenomena of the universe, several attempts have been made in recent years to model them from observations. Parameterization of cosmological or DE parameters is one of the most concerned attempts. One can parameterize the Hubble parameter, the deceleration parameter or the energy density of DE.[37,39–46] Parameterizing the DE density parameter, for example, using a simple power law expansion $\Omega_{\rm DE} = \sum_{i=0}^{N} A_i z^i$, where z is the red shift, is also a frequently used method.[47–53] Following this approach, one can parameterize the equation of state (EoS) of the DE as $w(z) = \sum_{i=0}^{N} w_i z^i$,[54–57] which is a simple parameterization of the EoS that can describe the dynamical evolutionary behavior for a large number of DE models. However, this parameterization diverges at high redshifts. Furthermore, since the angular diameter distance depends on the form of $w(z)$ and the angular scale features of the CMB temperature anisotropy varies with the peak, the constraint on the angular diameter distance to the last scattering surface by the CMB would be problematic. Then, a stable parameterization of the EoS $w(z) = w_0 + w_1 z/(1+z)$ that extends the parameterization of the DE to redshifts $z \gg 1$ was given and has been widely discussed.[58–66] Furthermore, a modified model $w(z) = w_0 + w_1 z/(1+z)^2$ was proposed by Jassal *et al.*[66] It can model a DE component that has the same value of EoS at the present time and at high redshifts. Both models are bounded at high redshifts $z \gg 1$, but they cannot be distinguished. In Ref. [63], Gong *et al.* also proposed two one-parameter models and the model $w(z) = w_0 \mathrm{e}^{z/(1+z)}/(1+z)$ such that $w = 0$ in the future $z \to -1$. Feng *et al.*[67] proposed two-parameter models $w(z) = w_0 + \frac{w_1 z}{1+z^2}$ and $w(z) = w_0 + \frac{w_1 z^2}{1+z^2}$, with $w(z)$ bounded in the future for both models. In Ref. [68], the authors classified the parameterized EoS models proposed in recent years by the number of parameters and gave the range of model parameters using numerical analysis. In the appendix of Ref. [69], the authors made a summary of various parameterized models in recent years. In our work, we aim to explore the cosmological feasibility of some DE models with parameterized EoS using recent observations to constrain the models.

A large number of DE models may produce similar evolutionary behaviors and, correspondingly, similar histories of cosmic expansion. Therefore, effective differentiation of models is very important. Using various data to test

*Corresponding authors. Email: fengcj@shnu.edu.cn; zhaixh@shnu.edu.cn
© 2023 Chinese Physical Society and IOP Publishing Ltd

DE models, to select good models, or to compare models, has become a standard approach in cosmological research. However, by using only one kind of observational data to constrain models, a degeneracy of certain cosmological parameter among different models usually occurs. In order to break this degeneracy, joint constraints of multiple observational data are often used. In our work, we will use the combination of supernova data, the temperature and polarization anisotropy data from the CMB, the baryon acoustic oscillations (BAO), and Hubble parameter observational $H(z)$ data. For supernova data, we will compare the constraints from two samples: joint light-curve analysis (JLA) and Pantheon, where the redshift range is extended in the latter.

In this Letter, we use the above-mentioned observational data to investigate the cosmological feasibility of six DE models with parameterized EoS,[59,63,66,67] and analyze the DE nature with geometric diagnostics. Firstly, six parametric DE models are reviewed. Secondly, we give the constraints of the models with observational data. Thirdly, we perform two diagnostic analyses that can distinguish the models, and analyze the impact of DE on the matter density perturbation by the growth factors of the models. Finally, we conclude our study.

Considered Six Parameterized Dark Energy Models. According to Einstein's gravitational field equation and the flat Fridmann–Robertson–Walker (FRW) metric, the Friedmann equations can be written as

$$\begin{aligned} 3H^2 &= \rho_{\rm m} + \rho_{\rm r} + \rho_{\rm de}, \\ 3H^2 + 2\dot{H} &= -(p_{\rm m} + p_{\rm r} + p_{\rm de}), \end{aligned} \tag{1}$$

where $H = \dot{a}/a$ is the Hubble parameter, a is the scale factor, and the dot is the derivative with respect to cosmic time; ρ_i and p_i are the energy density and pressure with subscript $i = {\rm m}$, r, and de denoting matter, radiation and DE, respectively. Here, we use units $8\pi G = 1$.

Assuming that there is no interaction between dark matter and DE in the universe, we have the equations of energy conservation as follows:

$$\begin{aligned} \dot{\rho_{\rm de}} + 3H(1+w)\rho_{\rm de} &= 0, \\ \dot{\rho_{\rm m}} + 3H\rho_{\rm m} &= 0, \end{aligned} \tag{2}$$

and it is assumed that the matter in the universe is dusty matter with $p_{\rm m} = 0$.

Firstly, we give a review of the six parameterized DE models that we will consider in the following.

Model 1: It was proposed by Gong and Zhang[63] with the EoS that

$$w\,(z) = \frac{w_0}{1+z}, \tag{3}$$

where the only parameter w_0 is constant. For this model, $w(z \to 0) = w_0$ is the current value of the EoS. The model is bounded by $w \sim 0$ at high redshift $z \gg 1$, which means that, at that time, DE is represented as dust matter. However, in the future $w(z \to -1) \sim \infty$, this model will have singularity. Combining Eqs. (1), (2), and (3), one obtains

$$\begin{aligned} E^2(z) = {} & (1 - \Omega_{\rm m0} - \Omega_{\rm r0})(1+z)^3 {\rm e}^{\frac{3w_0 z}{1+z}} \\ & + \Omega_{\rm m0}(1+z)^3 + \Omega_{\rm r0}(1+z)^4, \end{aligned} \tag{4}$$

where $E = H/H_0$ is the dimensionless Hubble parameter, H_0 is the current value of the Hubble constant. $\Omega_{i0} = \frac{\rho_{i0}}{3H_0^2}$ are the current values of density parameters.

Model 2: It is also a one-parameter model proposed by Gong and Zhang,[63] and its EoS is

$$w\,(z) = \frac{w_0}{1+z} {\rm e}^{\frac{z}{1+z}}. \tag{5}$$

Compared with Model 1, the EoS in the future $z \to -1$ for Model 2 is $w \to 0$, where DE represents dust matter. Similarly, one can obtain

$$\begin{aligned} E^2(z) = {} & (1 - \Omega_{\rm m0} - \Omega_{\rm r0})(1+z)^3 {\rm e}^{3w_0({\rm e}^{\frac{z}{1+z}} - 1)} \\ & + \Omega_{\rm m0}(1+z)^3 + \Omega_{\rm r0}(1+z)^4. \end{aligned} \tag{6}$$

Model 3: For two-parameter models, the parameterized EoS can be expressed as

$$w\,(z) = \frac{p}{\rho} = w_0 + w_1 f(z), \tag{7}$$

where w_0, w_1 are constants, and $f(z)$ is a function of the redshift z. Different forms of $f(z)$ correspond to different DE models. Also, the model will return to the ΛCDM model when $w_0 = -1$ and $w_1 = 0$.

The model with $f(z) = \frac{z}{1+z}$ is known as the Chevallier–Polarski–Linear (CPL) model,[59]

$$w(z) = w_0 + \frac{w_1 z}{1+z}. \tag{8}$$

This model is divergent when describing future evolution. Similarly, one has

$$\begin{aligned} E^2(z) = {} & (1 - \Omega_{\rm m0} - \Omega_{\rm r0})(1+z)^{3(1+w_0+w_1)} {\rm e}^{\frac{-3w_1 z}{1+z}} \\ & + \Omega_{\rm m0}(1+z)^3 + \Omega_{\rm r0}(1+z)^4. \end{aligned} \tag{9}$$

This is the Model 3 we will consider.

Model 4: This model[66] is a modification of Model 3 and its EoS is as follows:

$$w\,(z) = w_0 + \frac{w_1 z}{(1+z)^2}, \tag{10}$$

which diverges in the future as Model 3. We can obtain

$$\begin{aligned} E^2(z) = {} & (1 - \Omega_{\rm m0} - \Omega_{\rm r0})(1+z)^{3(1+w_0)} {\rm e}^{\frac{3w_1 z^2}{2(1+z)^2}} \\ & + \Omega_{\rm m0}(1+z)^3 + \Omega_{\rm r0}(1+z)^4. \end{aligned} \tag{11}$$

Model 5: In Ref. [67], Feng *et al.* proposed two-parameter models that are different from the CPL model and can describe the evolutionary behavior of the universe from the past to the future. Model 4 is one of the models with

$$w(z) = w_0 + \frac{w_1 z}{1+z^2}. \tag{12}$$

Then,

$$\begin{aligned} E^2(z) = {} & (1 - \Omega_{\rm m0} - \Omega_{\rm r0})(1+z)^{3(1+w_0-\frac{1}{2}w_1)} {\rm e}^{\frac{3}{2}w_1 \arctan z} \\ & \cdot (1+z^2)^{\frac{3}{4}w_1} + \Omega_{\rm m0}(1+z)^3 + \Omega_{\rm r0}(1+z)^4. \end{aligned} \tag{13}$$

Model 6: It is another two-parameter model in Ref. [67] with the EoS

$$w(z) = w_0 + \frac{w_1 z^2}{1+z^2}. \tag{14}$$

Similarly, one has

$$E^2(z) = (1-\Omega_{\rm m0}-\Omega_{\rm r0})(1+z)^{3(1+w_0+\frac{1}{2}w_1)}{\rm e}^{-\frac{3}{2}w_1 \arctan z} \cdot (1+z^2)^{\frac{3}{4}w_1} + \Omega_{\rm m0}(1+z)^3 + \Omega_{\rm r0}(1+z)^4. \tag{15}$$

The behaviors of the EoSs of the above six models are listed in Table 1. Among these models, the EoSs of Models 1, 3 and 4 will be divergent at $z \to -1$. However, the divergence can be avoided in Models 2, 5 and 6. Moreover, for Models 1 and 2 when $w_0 = -1$, the EoSs are the same as that of ΛCDM at the present time. For Model 3, the EoS is the same as ΛCDM in the past and at present time when $w_0 = -1$ and $w_1 = 0$. The EoS of Model 4 is the same as ΛCDM in the past and at present time when $w_0 = -1$. Models 5 and 6 return to ΛCDM when $w_0 = -1$ and $w_1 = 0$.

Table 1. Behaviors of EoS parameters for different DE models.

Models	$w(z)$	$z=0$	$z\to\infty$	$z\to-1$
Model 1 [63]	$w(z)=\frac{w_0}{1+z}$	w_0	0	∞
Model 2 [63]	$w(z)=\frac{w_0}{1+z}{\rm e}^{\frac{z}{1+z}}$	w_0	0	0
Model 3 [59]	$w(z)=w_0+\frac{w_1 z}{1+z}$	w_0	w_0+w_1	∞
Model 4 [66]	$w(z)w_0+\frac{w_1 z}{(1+z)^2}$	w_0	w_0	∞
Model 5 [67]	$w(z)=w_0+\frac{w_1 z}{1+z^2}$	w_0	w_0	$w_0-\frac{w_1}{2}$
Model 6 [67]	$w(z)=w_0+\frac{w_1 z^2}{1+z^2}$	w_0	w_0+w_1	$w_0+\frac{w_1}{2}$

Data Constraints. The fast development of observational techniques has led to increasingly refined observational data and gradually increased constraints on DE models. Moreover, in order to break down the degeneracy in cosmological parameters among different models, the combination of multiple observational data is frequently used to give subtle constraints. Here, we constrain the DE models mentioned above with the Pantheon + CMB + BAO + $H(z)$ and the JLA + CMB + BAO + $H(z)$ data sets. The constraint results are used to distinguish or compare the models. A brief introduction to these datasets are given in the following.

Pantheon and JLA Sample. We use the Pantheon SNIa sample at redshifts of $0.01 < z < 2.3$,[70] which is a combination of Pan-STARRS1 (PS1), Sloan Digital Sky Survey (SDSS), Supernova Legacy Survey (SNLS), some low redshift data, and the Hubble Space Telescope (HST) sample of a total of 1048 supernovae. The JLA dataset contains a total of 740 SNIa at redshifts of $0.01 < z < 1$,[71] including several samples at low redshifts ($z < 0.1$), all three seasons of SDSS-II ($0.05 < z < 0.4$) and three years of SNLS ($0.2 < z < 1$).

Due to the linear relationship between the extreme luminosity of SNIa bursts with the color of the light and the rate of decrease of the light-change curve, they are treated as standard candles for the detection of cosmological distances in astronomical observations. The luminosity distance is expressed in astronomical observations by introducing a distance modulus $m_{\rm cor} - M$,[72,73] i.e.,

$$\mu = m_{\rm cor} - M = 5\log_{10}(d_{\rm L}/{\rm Mpc}) + 25, \tag{16}$$

where $m_{\rm cor}$ is the corrected magnitude in the Pantheon observable, $d_{\rm L} = (1+z)\int_0^z \frac{dz'}{H(z')} = (1+z)r(z)$ is the photometric distance and $r(z)$ is the co-movement distance. Therefore, the actual observed distance of SNIa modulus is

$$\mu_{\rm obs} = m_{\rm B} - M + \alpha x_1 - \beta c + \Delta_{\rm M} + \Delta_{\rm B}, \tag{17}$$

where $m_{\rm B}$ is the apparent magnitude in the B-band, M is the absolute magnitude of the SN in the B-band when the stretching parameter $x_1 = 0$ and the color parameter $c = 0$, α is the luminosity versus stretching coefficient, β is the luminosity versus color number, $\Delta_{\rm M}$ is a distance correction based on the host galaxy mass of the SN, and $\Delta_{\rm B}$ is a distance correction based on the deviation predicted from the simulation (for details, see Ref. [70]). The χ^2 for the SNIa dataset is

$$\chi^2_{\rm SNIa} = [\mu_i^{\rm obs} - \mu_i^{\rm th}(p)](\mathrm{Cov}_{\rm SN}^{-1})_{ij}[\mu_j^{\rm obs} - \mu_j^{\rm th}(p)], \tag{18}$$

where $p = (p_1, \ldots, p_n)$ is a vector of n fit parameters, $\mathrm{Cov}_{\rm SN}$ is the covariance matrix describing the systematic error of the supernova observations, $\mu_i^{\rm obs}$ and $\mu_i^{\rm th}$ are the observed and theoretical distance moduli, respectively.

Cosmic Microwave Background. Generally, three observables from cosmic microwave background (CMB) observations are used to constrain the cosmological model parameters: the redshift $z_* = 1048[1 + 0.00124(\Omega_{\rm b}h^2)^{-0.738}][1 + g_1(\Omega_{\rm m}h^2)^{g_2}]$ during the photon decoupling period, the position of the first peak in the temperature rise power spectrum $l_{\rm A} = (1+z_*)\frac{\pi D_{\rm A} z_*}{r_{\rm s}(z_*)}$, and the translation parameter $\Re \equiv \sqrt{\Omega_{\rm m}H_0^2}(1+z_*)D_{\rm A}(z_*)$.

The χ^2 of the CMB is

$$\chi^2_{\rm CMB} = \Delta p_i[\mathrm{Cov}^{-1}_{\rm CMB}(p_i, p_j)]\Delta p_j, \tag{19}$$

where $\Delta p_i = p_i - p_i^{\rm data}$, $p_i = \{l_{\rm A}, \Re, w_{\rm b}\}$, and $w_{\rm b} = \Omega_{\rm b}h^2$. Using the Planck 2018 [74] data including temperature (TT), the polarization (EE), the cross correlation of temperature, and polarization (TE) power spectra, where the low multipoles (low-ℓ) temperature Commander likelihood in TT, the low-ℓ SimAll likelihood in EE and the high multipoles (high-ℓ) part of Planck TT, TE, EE are contributed in the range $\ell \in [2, 2500]$, one can obtain the central value of $p_i^{\rm data}$ and the error in the 1σ confidence interval (the relevant results are given in Ref. [74]).

Baryon Acoustic Oscillations. Baryon acoustic oscillations (BAOs) are used in astronomical observations as a standard ruler for cosmological measurements of cosmic distances, and their data are analyzed from BAO eigenpower spectra or correlation functions in large scale surveys of galaxy clusters to extract the physical quantities: redshift and distance.

In the direction of sight there is

$$H(z) = \frac{c\cdot\delta z_{\rm s}(z)}{r_{\rm s}(z_d)}. \tag{20}$$

Here, $r_{\rm s}(z_d)$ is the co-moving acoustic horizon during the baryon towing period, and $\delta z_{\rm s}$ denotes the BAO characteristic redshift distance along the direction of sight with redshift z.

In the direction perpendicular to the line of sight there is

$$d_{\rm A}(z) = \frac{r_{\rm s}(z_d)}{\theta_{\rm s}(z)(1+z)}, \tag{21}$$

where $\theta_{\rm s}(z)$ denotes the angle at which the BAO feature is opened perpendicular to the line of the sight direction. The data of BAO features can now be directly measured out of the value of the effective distance $D_{\rm V}(z)$ corresponding to the redshift,

$$\begin{aligned} D_{\rm V}(z) &= \frac{r_{\rm s}(z_d)}{[\theta_{\rm s}(z)^2 \delta z_{\rm s}(z)]^{\frac{1}{3}}} \\ &= \Big[\frac{(1+z)^2 d_{\rm A}^2(z) cz}{H(z)}\Big]^{\frac{1}{3}}. \end{aligned} \tag{22}$$

The χ^2 of BAO is

$$\chi^2_{\rm BAO} = \Delta p_i [{\rm Cov}^{-1}_{\rm BAO}(p_i, p_j)] \Delta p_j. \tag{23}$$

In our work, we utilize BAO measurements from 6dFGS,[75] SDSS-MGS[76] and BOSS DR12[77] as published by Planck 2018 results.[74]

$H(z)$ Observational Data. The Hubble parameter can characterize the evolution rate of the universe, and to some extent, the size and age of the universe. With the progress of the observational techniques, the accuracy of the current value of the Hubble constant has greatly improved. We use in our analysis a total of 57 data points[78] from direct observations of $H(z)$, i.e., $H(z)$ observational data (OHD), by both the age differential measurement method and the BAO effect.

The χ^2 of the observed data for $H(z)$ is

$$\chi^2_{\rm OHD} = \sum_{i=1}^{57} \frac{[H_{\rm th} - H_{\rm obs}]^2}{\sigma^2_{H(z_i)}}. \tag{24}$$

The total χ^2 combining the above four datasets is

$$\chi^2_{\rm tot} = \chi^2_{\rm SNIa} + \chi^2_{\rm CMB} + \chi^2_{\rm BAO} + \chi^2_{\rm OHD}. \tag{25}$$

The minimum values of χ^2, i.e., the $\chi^2_{\rm min}$ values, reflect the goodness of fit for models. That is, the smaller $\chi^2_{\rm min}$ values indicate that the model can be better supported by the current observation data. Since the $\chi^2_{\rm min}$ values decrease as the number of the model parameters increases, it is unlikely to make a fair judgement on the merit of the model by the $\chi^2_{\rm min}$ values alone. Considering the influence of the number of parameters, we will compare the models by using two information criterions, Akaike information criteria (AIC)[79] and Bayes information criterion (BIC),[80]

$$\rm AIC = \chi^2_{min} + 2\,\mathit{K}, \tag{26}$$

$$\rm BIC = \chi^2_{min} + \mathit{K} ln \mathit{N}, \tag{27}$$

where K is the number of free parameters, and N is the total data points.

We use the Markov Chain Monte Carlo (MCMC) method to explore the parameter space of these six parametrized DE models mentioned above and fit the data using the Pydm package (https://github.com/shfengcj/pydm) written by our own group. Here, we use two sets of combined data, i.e., JLA + CMB + BAO + $H(z)$ (JCBH) and Pantheon + CMB + BAO + $H(z)$ (PCBH) data sets, to obtain the best-fit values of the parameters of different DE models and their 1σ to 2σ confidence levels. The results are given in Tables 2 and 3. One can see that the EoS parameter crosses -1 at a certain redshift in Models 3 and 6. Taking the best fit results from the JCBH data for instance, in Model 3, the value of the EoS parameter at $z = 0$ is $w_0 = -0.9$, and it becomes $w_0 + w_1 = -1.41$ at $z = \infty$. In Model 6, the value of the EoS parameter at $z = 0$ is $w_0 = -0.95$, and it becomes $w_0 + w_1 = -1.58$ at $z = \infty$. This crossing behavior of the EoS parameter cannot be realized in single field models such as quintessence models, but can be realized in two-field models (see Refs. [81,82] for more details).

Table 2. The best fit values of the model parameters and 1σ confidence level of Models 1,2 and ΛCDM model under two sets of combined data.

Parameter	ΛCDM		Model 1		Model 2	
	JCBH	PCBH	JCBH	PCBH	JCBH	PCBH
H_0	$68.26^{+0.45}_{-0.51}$	$68.31^{+0.47}_{-0.50}$	$70.97^{+1.16}_{-1.16}$	$69.86^{+0.99}_{-0.99}$	$69.20^{+1.18}_{-1.09}$	$68.90^{+0.97}_{-0.98}$
w_0			$-1.31^{+0.05}_{-0.05}$	$-1.26^{+0.04}_{-0.05}$	$-1.06^{+0.05}_{-0.05}$	$-1.04^{+0.04}_{-0.04}$
$\chi^2_{\rm min}$	720.06	1062.87	745.31	1090.19	725.20	1067.81

Table 3. The best fit values of the model parameters and 1σ confidence level of Models 3–6 under two sets of combined data.

Parameter	Model 3		Model 4		Model 5		Model 6	
	JCBH	PCBH	JCBH	PCBH	JCBH	PCBH	JCBH	PCBH
H_0	$67.94^{+1.30}_{-1.23}$	$68.24^{+1.01}_{-1.00}$	$68.31^{+1.21}_{-1.32}$	$68.33^{+1.04}_{-1.02}$	$68.17^{+1.32}_{-1.23}$	$68.37^{+1.08}_{-1.03}$	$67.84^{+1.27}_{-1.36}$	$68.21^{+1.03}_{-1.03}$
w_0	$-0.90^{+0.09}_{-0.09}$	$-0.95^{+0.09}_{-0.08}$	$-0.93^{+0.11}_{-0.11}$	$-0.97^{+0.12}_{-0.11}$	$-0.94^{+0.10}_{-0.10}$	$-0.98^{+0.09}_{-0.08}$	$-0.95^{+0.07}_{-0.07}$	$-0.97^{+0.05}_{-0.05}$
w_1	$-0.51^{+0.33}_{-0.45}$	$-0.34^{+0.39}_{-0.45}$	$-0.49^{+0.65}_{-0.76}$	$-0.26^{+0.75}_{-0.85}$	$-0.29^{+0.33}_{-0.38}$	$-0.14^{+0.33}_{-0.39}$	$-0.63^{+0.33}_{-0.44}$	$-0.50^{+0.33}_{-0.49}$
$\chi^2_{\rm min}$	719.07	1062.05	719.85	1062.60	719.49	1062.56	718.18	1061.53

For better analysis and comparison, the ΛCDM model is chosen as a reference. The $\chi^2_{\rm min}$ values reflect the goodness of fit, and we note that Model 6 has the smallest $\chi^2_{\rm min}$ value in Tables 2 and 3, which is supported by current observational data. The best-fit values of model parameters for Model 6 and 1σ to 2σ confidence level are given in Fig. 1 by using the PCBH data. However, as mentioned above, the $\chi^2_{\rm min}$ values are not suitable for comparing models because of the $\chi^2_{\rm min}$ values are affected by the number of parameters. Here, we use the difference of AIC between a certain DE model and the ΛCDM model, $\Delta{\rm AIC} = \Delta\chi^2_{\rm min} + 2\Delta K$, and the difference of BIC, $\Delta{\rm BIC} = \Delta\chi^2_{\rm min} + 2\Delta K \ln N$, to quantitatively compare the models. We show in Table 4 the comparison of the models using the two information criterions. It is noted that for Models 1–6, $\Delta{\rm AIC} > 2$ and $\Delta{\rm BIC} > 2$, then, according to Refs. [83–85], the best model is still the ΛCDM model.

The main difference between the two sets of combined data is that the covariance matrices of the two supernova samples, Pantheon and JLA, are analyzed differently. The covariance matrix in the JLA sample depends explicitly on the parameters α and β, so these two parameters must be added as additional parameters in the MCMC search. In contrast, for the Pantheon sample, they do not need to be changed during the MCMC search because the effects of α and β have been considered in the covariance calculation. As described in Ref. [86], the constraints of PCBH and JCBH are known to be in good agreement. We note that, although the PCBH datasets cover a larger range of redshifts, they still have poor constraints for w_1 of Models 3–5. Meanwhile, the PCBH constraint results show that for Models 3–6 compared to JCBH, the values of w_0 are more negative and the values of w_1 are less negative, which is consistent with the result of Ref. [87]. For Models 1 and 2, the fit results prefer to choose less negative values of w_0.

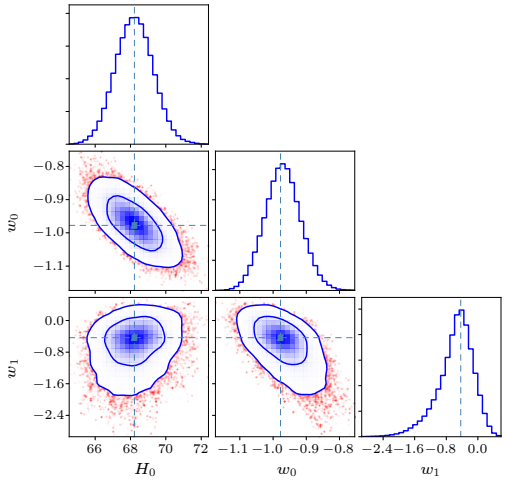

Fig. 1. Best-fit values of model parameters and their 1σ-to-2σ confidence levels for Model 6 by using the PCBH data.

Table 4. The results of AIC and BIC of PCBH data for the models.

Criterion	ΛCDM	Model 1	Model 2	Model 3	Model 4	Model 5	Model 6
AIC	1066.87	1096.16	1073.81	1070.05	1070.60	1070.56	1069.53
BIC	1076.89	1111.22	1088.84	1090.08	1090.63	1090.59	1089.56

Diagnostics of DE Models. So far, we are able to distinguish DE models from each other with observational constraints. With the purpose of investigating the cosmological behavior of various DE models and distinguishing one model from others, we will further use statefinder diagnostic, *Om* diagnostics, and growth factor to distinguish Models 1–6 from each other as well as from the ΛCDM, quintessence, and Chaplygin gas models.

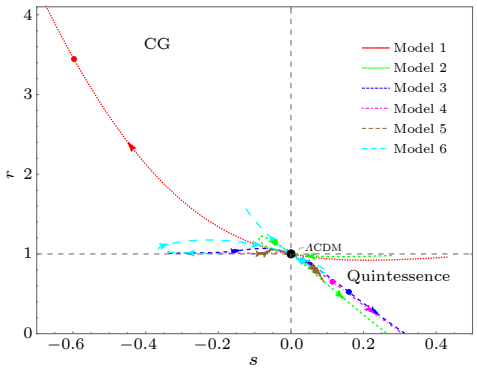

Fig. 2. Evolution trajectories of the six DE models in the r–s plane, where the arrows indicate the temporal evolution of these models. The solid dots on these lines indicate the current states of the models and the point (0,1) represents the ΛCDM model.

Statefinder Diagnostics. Sahni *et al.*[88,89] proposed a statefinder diagnostics $\{r, s\}$, which is a geometric-parametric method to distinguish different DE models. The parameters are defined as follows:

$$r = \frac{\dddot{a}}{aH^3}, \tag{28}$$

$$s = \frac{r - 1}{3(q - \frac{1}{2})}, \quad q \neq \frac{1}{2}, \tag{29}$$

where $q = -\frac{\ddot{a}}{aH^2}$ is the deceleration parameter.

Different (r, s) pairs correspond to different DE models.[88,89] For example,

- $(r = 1, s = 0) \rightarrow \Lambda$CDM model,
- $(r\langle 1, s\rangle 0) \rightarrow$ quintessence model,
- $(r > 1, s < 0) \rightarrow$ Chaplygin gas (CG) model.

According to the best-fit values given in Tables 2 and 3, we plot the evolution of the statefinder diagnostic parameter pair $\{r, s\}$ for the six DE models in Fig. 2, and also give the local enlargement in Fig. 3 for clarity. The arrows indicate the directions of evolution of the models. Moreover, we compare the six DE models with the CG and quintessence models and the ΛCDM model. It is found that Model 1 behaves like the quintessence model at early time, then makes transition from quintessence to ΛCDM

fixed point, and finally gets into the CG region. Model 2 behaves like quintessence at early time, and passes through the ΛCDM point as it evolves. After performing a swirl, it lies at quintessence region in the future. Model 5 is exactly the opposite. Its early evolution resembles the CG model, then crosses the ΛCDM point and swivels round, finally enters the CG region in the future. The evolutionary trajectories of Models 3, 4, and 5 are like the CG model at early time, then they cross the ΛCDM fixed point into quintessence region. However, the evolutionary trajectories of the two models do not overlap. Thus, the six DE models can be distinguished from each other and from the ΛCDM, CG, quintessence models by using the statefinder diagnostics method.

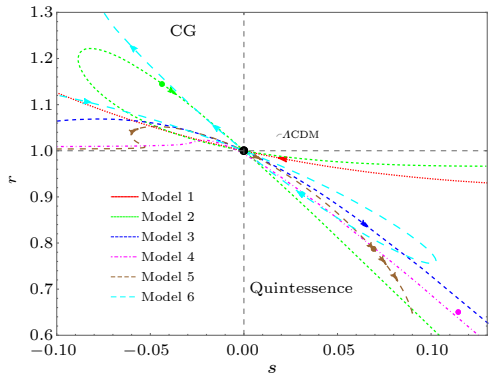

Fig. 3. The local enlargement of Fig. 2.

Om Diagnostics. Another diagnostic tool is often used to distinguish the DE models and to deeply understand the constructed cosmological models, called $Om(z)$ diagnostics.[90,91] $Om(z)$ is defined as

$$Om(z) = \frac{E^2(z) - 1}{(1+z)^3 - 1}. \tag{30}$$

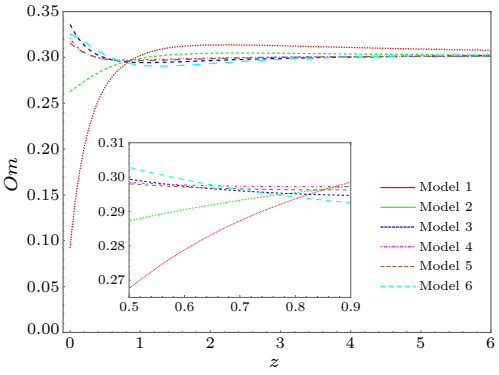

Fig. 4. Evolutions of the six DE models in Om–z plots.

The slope of $Om(z)$ can distinguish different DE models. The positive, negative and null slopes of $Om(z)$ correspond to phantom ($w < -1$), quintessence ($w > -1$) and ΛCDM ($w = -1$) models, respectively. In Fig. 4, we plot the evolution curves of $Om(z)$ to these six DE models by using the best-fit values given in Tables 2 and 3. None of these models have an evolution curve with a null slope. From the evolution trends of these six models in Fig. 4, we find that Models 2–6 are not significantly distinguishable in the early stage, but can be clearly distinguished at $z < 1$. It is obvious that the results of the $Om(z)$ diagnostic are consistent with the statefinder results.

Growth Factor. During the evolution of the universe, gravity can increase the amplitude of matter perturbations, especially at the period of matter dominance. DE not only accelerates the expansion of the universe, but also changes the growth rate of matter perturbations. On the other hand, different models possibly give the similar accelerated expansion at late time, but they may produce different growths of matter perturbations.[92–101] Therefore, in addition to using observational data to distinguish DE models, exploring the effect of the DE models on the growth rate of matter perturbations on large scales in the universe is another available way. Here we analyze the types of the six DE models by considering the growth rate of matter density perturbations. Assume that the fluid in the universe satisfies the continuity equation, Euler's equation, and Poisson's equation as follows:

$$\dot{\rho} + \nabla \cdot (\rho v) = 0, \tag{31}$$

$$\dot{v} + (v \cdot \nabla)v + \frac{1}{\rho}\nabla p + \nabla\phi = 0, \tag{32}$$

$$\nabla^2\phi = 4\pi G\rho, \tag{33}$$

where ϕ is the gravitational potential, ρ is the fluid density, p is the pressure, and v is the velocity of fluid motion. Assume that Eqs. (31)–(33) have perturbative solutions $\rho = \rho_0 + \delta\rho$, $v = v_0 + \delta v$, $p = p_0 + \delta p$, $\phi = \phi_0 + \delta\phi$. Introducing a new quantity $\delta(t, r) = \frac{\delta\rho}{\rho_{\rm m}} = \delta(t)\exp(ik \cdot x)$ and further assuming that the system is an adiabatic state, one can reach the linear perturbation equation

$$\ddot{\delta}(t) + 2H\dot{\delta}(t) - 4\pi G\rho_{\rm m}\delta(t) = 0. \tag{34}$$

From Eqs. (1) and (2), one has the evolutionary equation of the material density parameter $\Omega_{\rm m} = \frac{\rho_{\rm m}}{3H^2}$,

$$\frac{d\Omega_{\rm m}}{d\ln a} = 3w(1 - \Omega_{\rm m})\Omega_{\rm m}. \tag{35}$$

In general, the growth of perturbation is described by introducing a growth factor

$$f = \frac{d\ln\delta_+}{d\ln a}, \tag{36}$$

where δ_+ denotes the growth solution of the perturbation equation. Then, using Eqs. (35) and (36), the perturbation equation (34) can be rewritten as

$$\frac{df}{d\ln a} + f^2 + \left[\frac{1}{2} - \frac{3}{2}(1 - \Omega_{\rm m})w\right]f = \frac{3}{2}\Omega_{\rm m}. \tag{37}$$

We assume that the perturbation equation has a good approximate solution $f = \Omega_{\rm m}^{\gamma}$,[93–98] where γ is the growth index. Substituting $f = \Omega_{\rm m}^{\gamma}$ into Eq. (37) yields

$$3w(1 - \Omega_{\rm m})\Omega_{\rm m}\ln\Omega_{\rm m}\frac{d\gamma}{d\Omega_{\rm m}} - 3w\left(\gamma - \frac{1}{2}\right)\Omega_{\rm m} + \Omega_{\rm m}^{\gamma} - \frac{3}{2}\Omega_{\rm m}^{1-\gamma} + 3w\gamma - \frac{3}{2}w + \frac{1}{2} = 0. \tag{38}$$

Ignoring radiation, we have $\Omega_{\rm m} + \Omega_{\rm de} = 1$. Setting a new variable $x = 1 - \Omega_{\rm m}$, taking the Taylor expansion of

Eq. (38) near $x = 0$ and letting $\gamma = \gamma_0 + \gamma_1 x + \gamma_2 x^2 + \cdots$, we can obtain the growth index as follows:[93,94]

$$\gamma = \frac{3(1-w)}{5-6w} - \frac{3(w-1)(3w-2)}{2(5-6w)^2(12w-5)}x - \frac{(w-1)(-194+1131w-1908w^2+972w^3)}{4(5-6w^4)(12w-5)}x^2 + o(x^3). \quad (39)$$

From Eq. (39), it is clear that the value of γ is model-dependent. The EoS of the ΛCDM model is a constant $w = -1$, then $\gamma \approx 0.554698$. Based on the best-fit values in Tables 2 and 3, we give the growth index of each model as a function of redshift, as shown in Fig. 5. Furthermore, we plot in Fig. 6 the relative error $\sigma = \frac{f_{\Lambda\mathrm{CDM}} - f_{\mathrm{Model}}}{f_{\mathrm{Model}}}$ [94] of the growth factor approximation between the ΛCDM model and all the other DE models. We note that although approximations of $f_{\Lambda\mathrm{CDM}}$ and f_{Model} are very close to relative errors in the thousands of parts, we can still distinguish the six DE models from the ΛCDM model.

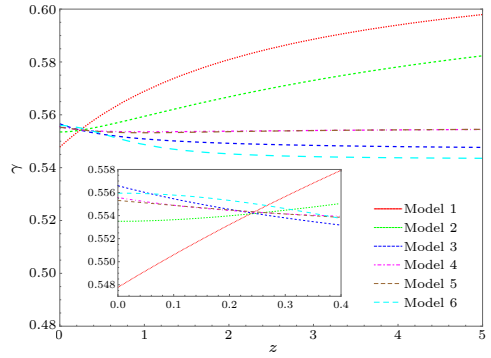

Fig. 5. The evolution of growth index with redshift in different DE models.

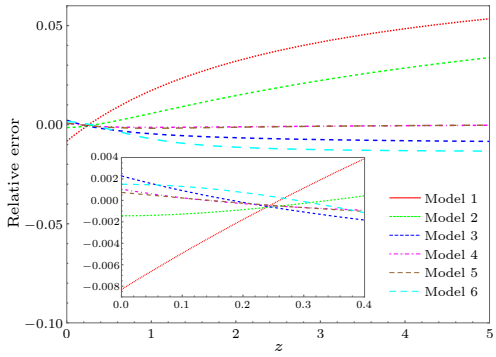

Fig. 6. Evolution of relative errors of the growth factor approximation between the ΛCDM model and the different DE models with redshift.

Conclusion and Discussion. In the face of many kinds of DE models, the observation data play an extremely important role to constrain the parameter space of the DE models. In this work, we mainly use two sets of combined data: JLA + CMB + BAO + OHD (JCBH) and Pantheon + CMB + BAO + OHD (PCBH) to constrain the six parameterized DE models. The fitting results of the two combined datasets indicate that Models 3–6 are supported by recent observations, whereas the AIC and BIC results show that ΛCDM is still the best model. Hence, it is feasible to use the observational data to effectively distinguish and compare the DE models. Comparing the PCBH with the JCBH, we find that, though covering a larger redshift range, the PCBH still has poor constraints and broadens the uncertainty of the model parameters, and is also unable to relieve the H_0 tension. The reason may be in the precision and the numbers of the observed data. As is known, large redshift data points have larger relative errors than small redshift data points. Therefore, although the PCBH data cover a larger redshift range, they give poor constraints on model parameters (see Ref. [87] for detailed discussion). Then we expect more measurement results to help solve this problem, as mentioned in Ref. [102].

We also use some geometrical methods to distinguish the DE models. By using statefinder and Om diagnostics, we can distinguish the six parameterized models from each other and from the ΛCDM, CG, and quintessence models. The two diagnostic results are consistent. In addition, we analyze the growth factors of the matter density perturbations of the six DE models and compare them with the ΛCDM model. The results show that these DE models can be clearly distinguished. Actually, direct parameterization of growth factor or growth index can also be used to understand the properties of DE,[94,103–108] and observational constraints may further distinguish different models. This issue is worth further study in the future by considering new forms of parameterization and using more new observational data.

The problems of H_0 tension and σ_8 tension are very important in modern cosmology. In this study, we mainly focus on testing and performing constraints on some parameterized dark energy models with latest data. The H_0 tension does not seem to be relieved in these models. The best fitting value for H_0 is around 67.84–70.97 with 1σ confidence about ± 1.0. It means that one needs some mechanism to alleviate the H_0 tension for these models. The root-mean-square amplitude of matter perturbations[109] σ_8 also has tension between the result from the low-redshift probes such as the weak gravitational lensing and galaxy clustering and the value from CMB observations.[109,110] A way to solve this problem is to introduce a friction between dark matter and dark energy[111] (see Ref. [112] for other possible solutions). The models discussed here are lack of corresponding methods to alleviate this problem. The problems of H_0 tension and σ_8 tension are worthy of deep study for the parameterized dark energy models and we leave them to our next work.

Acknowledgment. This work was supported by the National Natural Science Foundation of China (Grant No. 11105091).

References

[1] Perlmutter S *et al.* [Supernova Cosmology Project] 1999 *Astrophys. J.* **517** 565

[2] Riess A G *et al.* [Supernova Search Team] 1998 *Astron. J.* **116** 1009

[3] Tegmark M *et al.* [SDSS] 2004 *Phys. Rev. D* **69** 103501
[4] Seljak U *et al.* [SDSS] 2005 *Phys. Rev. D* **71** 103515
[5] Bennett C L *et al.* [WMAP] 2003 *Astrophys. J. Suppl.* **148** 1
[6] Spergel D N *et al.* [WMAP] 2007 *Astrophys. J. Suppl.* **170** 377
[7] Spergel D N *et al.* [WMAP] 2003 *Astrophys. J. Suppl.* **148** 175
[8] Ade P A R *et al.* [Planck] 2011 *Astron. Astrophys.* **536** A14
[9] Ade P A R *et al.* [Planck] 2011 *Astron. Astrophys.* **536** A1
[10] Ade P A R *et al.* [Planck] 2011 *Astron. Astrophys.* **536** A2
[11] Nojiri S and Odintsov S D 2006 *Int. J. Geometr. Methods Mod. Phys.* **04** 115
[12] De Felice A and Tsujikawa S 2010 *Living Rev. Relativ.* **13** 3
[13] Capozziello S and De Laurentis M 2011 *Phys. Rep.* **509** 167
[14] Cai Y F, Capozziello S, De Laurentis M, and Saridakis E N 2016 *Rept. Prog. Phys.* **79** 106901
[15] Carroll S M 2001 *Living Rev. Relativ.* **4** 1
[16] Peebles P J E and Ratra B 2003 *Rev. Mod. Phys.* **75** 559
[17] Bartelmann M 2010 *Rev. Mod. Phys.* **82** 331
[18] Sahni V 2004 *Lecture Notes in Physics* (Berlin: Springer) vol 653 p 141
[19] Copeland E J, Sami M, and Tsujikawa S 2006 *Int. J. Mod. Phys. D* **15** 1753
[20] Li M, Li X D, Wang S, and Wang Y 2011 *Commun. Theor. Phys.* **56** 525
[21] Li M, Li X D, Wang S, and Wang Y 2013 *Front. Phys.* **8** 828
[22] Frieman J, Turner M, and Huterer D 2008 *Ann. Rev. Astron. Astrophys.* **46** 385
[23] Straumann N 2006 *Mod. Phys. Lett. A* **21** 1083
[24] Weinberg S 2000 arXiv: astro-ph/0005265
[25] Guo Z K and Zhang Y Z 2005 *Phys. Rev. D* **71** 023501
[26] Guo Z K, Cai R G, and Zhang Y Z 2005 *J. Cosmol. Astropart. Phys.* **2005(05)** 002
[27] Guo Z K, Ohta N, and Tsujikawa S 2007 *Phys. Rev. D* **76** 023508
[28] Yang T, Guo Z K, and Cai R G 2015 *Phys. Rev. D* **91** 123533
[29] Ratra B and Peebles P J E 1988 *Phys. Rev. D* **37** 3406
[30] Zlatev I, Wang L M, and Steinhardt P J 1999 *Phys. Rev. Lett.* **82** 896
[31] Brax P and Martin J 2000 *Phys. Rev. D* **61** 103502
[32] Barreiro T, Copeland E J, and Nunes N J 2000 *Phys. Rev. D* **61** 127301
[33] Garriga J and Mukhanov V F 1999 *Phys. Lett. B* **458** 219
[34] Caldwell R R 2002 *Phys. Lett. B* **545** 23
[35] Caldwell R R, Kamionkowski M, and Weinberg N N 2003 *Phys. Rev. Lett.* **91** 071301
[36] Sola J and Štefančić H 2005 *Phys. Lett. B* **624** 147
[37] Roy N, Goswami S, and Das S 2022 *Phys. Dark Univ.* **36** 101037
[38] Yang W, Pan S, Di Valentino E, Saridakis E N, and Chakraborty S 2019 *Phys. Rev. D* **99** 043543
[39] Özer M and Taha M O 1987 *Nucl. Phys. B* **287** 776
[40] Abdel-Rahman A M M 1990 *Gen. Rel. Gravit.* **22** 655
[41] Vishwakarma R G, A, and Beesham A 1999 *Phys. Rev. D* **60** 063507
[42] Vishwakarma R G 2001 *Gen. Rel. Gravit.* **33** 1973
[43] A and Prajapati S R 2011 *Chin. Phys. Lett.* **28** 029803
[44] Pacif S K J and A 2014 *Eur. Phys. J. Plus* **129** 244
[45] Mamon A A 2018 *Mod. Phys. Lett. A* **33** 1850113
[46] Rezaei M, Malekjani M, and Sola J 2019 *Phys. Rev. D* **100** 023539
[47] Alam U, Sahni V, Saini T D, and Starobinsky A A 2004 *Mon. Not. Roy. Astron. Soc.* **354** 275
[48] Alam U, Sahni V, and Starobinsky A A 2004 *J. Cosmol. Astropart. Phys.* **2004(06)** 008
[49] Daly R A and Djorgovski S G 2003 *Astrophys. J.* **597** 9
[50] Daly R A and Djorgovski S G 2004 *Astrophys. J.* **612** 652
[51] Gong Y G 2012 *Int. J. Mod. Phys. D* **14** 599
[52] Jonsson J, Goobar A, Amanullah R, and Bergstrom L 2004 *J. Cosmol. Astropart. Phys.* **2004(09)** 007
[53] Alam U, Sahni V, Saini T D, and Starobinsky A A 2004 arXiv:astro-ph/0406672 [astro-ph]
[54] Weller J and Albrecht A 2001 *Phys. Rev. Lett.* **86** 1939
[55] Huterer D and Turner M S 2001 *Phys. Rev. D* **64** 123527
[56] Weller J and Albrecht A 2002 *Phys. Rev. D* **65** 103512
[57] Astier P 2001 *Phys. Lett. B* **500** 8
[58] Chevallier M and Polarski D 2001 *Int. J. Mod. Phys. D* **10** 213
[59] Linder E V 2003 *Phys. Rev. Lett.* **90** 091301
[60] Choudhury T R and Padmanabhan T 2005 *Astron. Astrophys.* **429** 807
[61] Feng B, Wang X L, and Zhang X M 2005 *Phys. Lett. B* **607** 35
[62] Gong Y G 2005 *Class. Quantum Grav.* **22** 2121
[63] Gong Y G and Zhang Y Z 2005 *Phys. Rev. D* **72** 043518
[64] Yang W, Pan S, Di Valentino E, and Saridakis E N 2019 *Universe* **5** 219
[65] Escamilla L A, and Vazquez J A 2021 arXiv:2111.10457 [astro-ph.CO]
[66] Jassal H K, Bagla J S, and Padmanabhan T 2005 *Mon. Not. Roy. Astron. Soc.* **356** L11
[67] Feng C J, Shen X Y, Li P, and Li X Z 2012 *J. Cosmol. Astropart. Phys.* **2012(09)** 023
[68] Perković D and Štefančić H 2020 *Eur. Phys. J. C* **80** 629
[69] Pacif S K J 2020 *Eur. Phys. J. Plus* **135** 792
[70] Scolnic D M *et al.* [Pan-STARRS1] 2018 *Astrophys. J.* **859** 101
[71] Betoule M *et al.* [SDSS] 2014 *Astron. Astrophys.* **568** A22
[72] Gao C, Chen Y, and Zheng J 2020 *Res. Astron. Astrophys.* **20** 151
[73] Xu T, Chen Y, Xu L, and Cao S 2022 *Phys. Dark Univ.* **36** 101023
[74] Aghanim N *et al.* [Planck] 2020 *Astron. Astrophys.* **641** A5
[75] Beutler F, Blake C, Colless M, Jones D H, Staveley-Smith L, Campbell L, Parker Q, Saunders W, and Watson F 2011 *Mon. Not. Roy. Astron. Soc.* **416** 3017
[76] Ross A J, Samushia L, Howlett C, Percival W J, Burden A M M 2015 *Mon. Not. Roy. Astron. Soc.* **449** 835
[77] Chuang C H *et al.* [BOSS] 2017 *Mon. Not. Roy. Astron. Soc.* **471** 2370
[78] Sharov G S and Vasiliev V O 2018 *Math. Model. Geom.* **6** 1
[79] Akaike H 1974 *IEEE Trans. Automat. Control* **19** 716
[80] Schwarz G 1978 *Ann. Statist.* **6** 461
[81] Guo Z K, Piao Y S, Zhang X M, and Zhang Y Z 2005 *Phys. Lett. B* **608** 177
[82] Guo Z K, Piao Y S, Zhang X M, and Zhang Y Z 2006 *Phys. Rev. D* **74** 127304
[83] Kass R E and Raftery A E 1995 *J. Am. Statist. Assoc.* **90** 773
[84] Xu Y Y and Zhang X 2016 *Eur. Phys. J. C* **76** 588

[85] Rezaei M 2019 *Mon. Not. Roy. Astron. Soc.* **485** 550
[86] Jones D O, Scolnic D M, Riess A G *et al.* 2018 *Astrophys. J.* **857** 51
[87] Di Valentino E, Gariazzo S, Mena O, and Vagnozzi S 2020 *J. Cosmol. Astropart. Phys.* **2020(07)** 045
[88] Alam U, Sahni V, Saini T D, and Starobinsky A A 2003 *Mon. Not. Roy. Astron. Soc.* **344** 1057
[89] Sahni V, Saini T D, Starobinsky A A, and Alam U 2003 *JETP Lett.* **77** 201
[90] Sahni V, Shafieloo A, and Starobinsky A A 2008 *Phys. Rev. D* **78** 103502
[91] Zunckel C and Clarkson C 2008 *Phys. Rev. Lett.* **101** 181301
[92] Starobinsky A A 1998 *JETP Lett.* **68** 757
[93] Wang L M and Steinhardt P J 1998 *Astrophys. J.* **508** 483
[94] Gong Y G, Ishak M, and Wang A Z 2009 *Phys. Rev. D* **80** 023002
[95] Peebles P J E 1980 *The Whole Truth: A Cosmologist's Reflections on the Search for Objective Reality* (New Jersey: Princeton University Press)
[96] Fry J N 1985 *Phys. Lett. B* **158** 211
[97] Silveira V and Waga I 1994 *Phys. Rev. D* **50** 4890
[98] Gong Y G 2008 *Phys. Rev. D* **78** 123010
[99] Gannouji R and Polarski D 2008 *J. Cosmol. Astropart. Phys.* **2008(05)** 018
[100] Nesseris S and Perivolaropoulos L 2008 *Phys. Rev. D* **77** 023504
[101] Polarski D, Starobinsky A A, and Giacomini H 2016 *J. Cosmol. Astropart. Phys.* **2016(12)** 037
[102] Ivezić Ž, Kahn S M, Tyson J A *et al.* [LSST] 2019 *Astrophys. J.* **873** 111
[103] Wu P, Yu H W, and Fu X 2009 *J. Cosmol. Astropart. Phys.* **2009(06)** 019
[104] Jing J L and Chen S B 2010 *Phys. Lett. B* **685** 185
[105] Bueno B A, Garcia-Bellido J, and Sapone D 2011 *J. Cosmol. Astropart. Phys.* **2011(10)** 010
[106] Gupta G, Sen S, and Sen A A 2012 *J. Cosmol. Astropart. Phys.* **2012(04)** 028
[107] Mehrabi A 2018 *Phys. Rev. D* **97** 083522
[108] Velásquez-Toribio A M and Fabris J C 2020 *Eur. Phys. J. C* **80** 1210
[109] Aghanim N, Akrami Y, Ashdown M *et al.* [Planck] 2020 *Astron. Astrophys.* **641** A6 [Erratum: *Astron. Astrophys.* **652** C4]
[110] Douspis M, Salvati L, and Aghanim N 2018 *Proc. Sci.* **335** 037
[111] Poulin V, Bernal J L, Kovetz E, and Kamionkowski M 2022 arXiv:2209.06217 [astro-ph.CO]
[112] Escudero H G, Kuo J L, Keeley R E, and Abazajian K N 2022 arXiv:2208.14435 [astro-ph.CO]